ANALYSIS AND OPTIMIZATION ON THE PROCESS OF ADJUSTABLE DOUBLE DRUM CASTOR SHELLING BASED ON DISCRETE ELEMENT METHOD

/

基于离散元的可调式双滚筒蓖麻脱壳过程分析及优化

Hou Junming, Zhu Hongjie, Jinpeng Li, Enchao Yao, Hu Weixue [1]
Shenyang Agricultural University, College of Engineering / China;
Tel: +86024-88487119 E-mail: junming_hou@163.com
DOI: https://doi.org/10.35633/inmateh-62-30

Keywords: *castor, stress analysis, size optimization, shelling machine, DEM*

ABSTRACT

The shelling stress of the castor capsule is difficult to obtain by experiments, which is vital for the design of the key components for the shelling machine. The stress analysis of the shelling process of the castor capsule is carried out. In this study, the typical variety castor Tongbi 11 is taken as the research object, and the model of castor shelling is established. The stress and rate of shelling removal of the inner drum are analysed. The effects of size optimization on the shelling results were analysed. The shelling machine was designed for the experiment. In the condition of the highest rate of shelling, the size of the outer drum is maintained, and the inner drum angle is 4.5. The length of the drum is 605mm. At this time, the shelling rate is 96.42 %, which is 0.39 % different from the fitting value. This study provides theoretical support for the design and parameter optimization of the castor shelling machine and its key components.

摘要

蓖麻蒴果的脱壳应力难以通过实验获得，这对脱壳机关键部件的设计非常重要。本研究对蓖麻蒴果脱壳过程进行了应力分析并对关键部件进行优化。本研究以典型品种通蓖11号为研究对象，建立了脱壳模型。分析脱壳的应力和脱壳率。得到蓖麻蒴果各阶段的最大压力、内外滚筒压力。分析尺寸优化结果对脱壳效果的影响，并设计试验台进行试验。结果表明，脱壳率最高的情况下，保持外筒尺寸不变，内筒角度为4.5°。滚筒的长度为605㎜。此时脱壳率为96.42%，与拟合值相差0.39%。本研究为蓖麻脱壳关键部件的设计和参数优化提供了理论支持。

INTRODUCTION

Castor is one of the ten oil crops in the world. Its oil is a crucial lubricating oil for aerospace, railway, and high-speed machine tools (*Li Jinqin et al., 2004; Hou J.M., et al., 2020; Huang Zhihui et al., 2013; Liu Rukuan et al., 2015*). Shelling is the first step of castor oil processing, which directly affects the quality of subsequent products. The existing shelling machine is low efficiency and high shelling damage rate, which reduces the quality of castor oil. (*Sebastian Romuli et al., 2015; Bo Yuan Lim et al., 2014; Boyuan L. et al., 2015*). The principles of the force properties among particles in the process of shelling are not clear, which leads to the unclear mechanism of shelling damage. The discrete element method can be applied to study the principles of group force in the process of shelling, which enrich the design theory of castor oil shelling equipment.

Some scholars (*Wang Zhibing et al., 2015; Ali Nejat Lorestani et al., 2013; Hou Junming et al., 2015*) explored the mechanical properties of agricultural material and analysed its rupture principle. *Mehrdad et al., (2016),* took corn as the research object, constructed two different models, explained the movement and mixing of corn in the machine, and compared with the experiment results. *Coetzee* et al., *(2016),* calibrated a gravel particle model, which established the gravel particle composed of 2, 4, and 8 particles, and compared the results with the resting angle calibration. Some scholars *(Jia Honglei et al., 2018; Zhao Shuhong et al., 2016; Shi Song et al., 2015; Dun Guoqiang* et al*., 2016)* used discrete element method to analyse the movement of particles in the seeder and compared the seeding rate, seeding leakage rate and reseeding rate were obtained by simulation analysis with the experiment.

[1] *Hou Junming, Associate Prof., Ph.D. Eng.; Zhu Hongjie., MS. Stud. Eng.; Li jinpeng, MS. Stud. Eng.; Yao Enchao, MS. Stud. Eng.; Hu Weixue, MS. Stud. Eng.*

The EDEM software was applied to study the stress on the lining board of a ball mill and analysed the interaction between pulp and coarse particles (*Sun Shanshan et al., 2018; Hao Wanjun et al., 2010; Bian Xiaolei et al., 2017; Li Kunyuan et al., 2017; Cleary P W et al., 2015;* and *Sinnott M D et al., 2017*). The key discrete element parameters of soil were calculated and the stress condition of the rotary blade under different working conditions were studied (*Wang et al., 2017; Wu Tao et al., 2017; Xiong Pingyuan et al., 2017;* and *Xiong Pingyuan et al., 2018)*. That provides a reference for studies on rotary tillage, energy consumption, and blade wear. In conclusion, the research on the mechanical properties of agricultural material has made specific progress, but there are a few studies on the force analysis of the group moved in the process of shelling of particles, especially on the force between particles and shelling parts, and the force between them. We take the typical variety castor Tongbi 11 as the research object. The pressure, speed, shelling clearance, and internal drum filling amount are studied. The influence of the stress and shelling rate in the process of shelling was analysed. Experiments were applied to verify the simulation results. This study can provide theoretical support for the design of the castor shelling machine and its key components.

MATERIALS AND METHODS

Hertz-Mindlin bonding contact model

In this study, a castor bond model is established. In the model, the relationship between the force and displacement of particles in each contact is described by six parameters, including the stiffness and tangential stiffness, and the friction coefficient between two contact particles. The particle to particle contact, the centre of the contact area, the line between the centre point of two particles, and the centre point are established.

Establishment of a castor capsule fragmentation model

We established the castor discrete model, and the contact model is by Hertz-Mindlin model. The whole particle is composed of three particles, which are combined by bonding to form a single castor capsule. Fig 1 is the model replacement model. Table 1 is the primary setting of parameters for the castor discrete element, and Table 2 is the setting of bonding parameters.

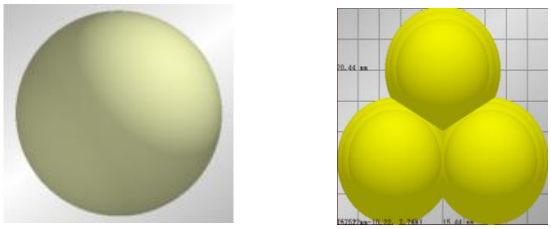

(a)Model before replacement *(b) Model after replacement*

Fig. 1 - Replacement effect of castor discrete element model

Parameters setting of castor discrete element model **Table 1**

Category	Value	Category	Value	Category	Value
Castor Poisson's ratio	0.3	Q235 steel Poisson's ratio	0.3	Rubber Poisson's ratio	0.45
Castor shear modulus [10^3MPa]	17	Q235 steel shear modulus [10^3MPa]	79	Rubber shear modulus [10^3MPa]	1
Castor density [kg/m^3]	1000	Steel density Q235[kg/m^3]	7800	Rubber density[kg/m^3]	9100
Castor - castor collision recovery coefficient	0.15	Collision recovery coefficient of castor-Q235 steel	0.44	Castor-rubber collision recovery coefficient	0.37
Castor - castor static friction coefficient	0.6	Static friction coefficient of castor-Q235 steel	0.4	Castor-rubber static friction coefficient	0.7
Castor oil - castor oil dynamic friction coefficient	0.05	Dynamic friction coefficient of castor-Q235 steel	0.01	Castor-rubber coefficient of kinetic friction	0.05

Table 2

Setting of bonding parameters

Bonding parameters		Value
Unit area normal stiffness	[N/m^3]	2.1×10^9
Tangential stiffness per unit area	[N/m^3]	1.4×10^9
Maximum normal force	[Pa]	2.1×10^6
Maximum tangential force	[Pa]	1.5×10^6
Bond plate radius	[mm]	1.6

Establishment of castor capsule shelling model

It is known from the mechanical properties of the castor capsule (*Fang Huimin et al., 2017*) that when castor capsule is ruptured and unshelled, three-compartment separation is carried out firstly, and then single-compartment capsule is unshelled. When the three-compartment structure is destroyed, then it moves to the rubbing and pressing area for shelling. The six pressing pieces are welded at the shelling drum, which is distributed evenly on the inner drum. The pressing pieces are coated with 3.0mm thick mesh rubber. Fig.2 shows the model and the inner drum model, and Table 3 shows the parameters of the shelling machine model.

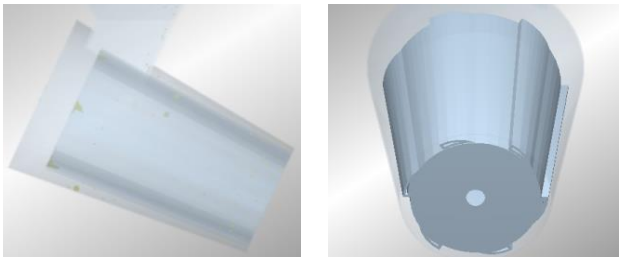

(a)Shelling model *(b) Inner drum model*

Fig. 2 - Shelling model and inner drum model

Setting of shelling machine parameters **Table 3**

Name		Value	Name		Value
Minimum radius of the inner drum	[mm]	137	The roller cone angle	[°]	4
Minimum radius of the outer drum	[mm]	158	Outside of the roller cone angle	[°]	5.5
Inner drum length	[mm]	600	Inlet length	[mm]	300
Length of outer drum	[mm]	700	Inlet width	[mm]	200
Drum angle	[°]	25	Pressure height	[mm]	12
The end arc length of the pressing sheet outlet	[mm]	79	Big end arc length	[mm]	100

Setting and results of the simulation

The response values of pressure and decanting rate of the inner drum were taken as the response values. Response surface analysis was carried out according to the results. Table 4 is the factor level for simulation.

Test factor level of Box-Benhnken **Table 4**

Level	A Speed	B Shelling gap	C Filling amount
	[r/min]	[mm]	[%]
-1	250	5.0	30
0	300	6.0	40
1	350	7.0	50

RESULTS

Analysis of inner drum stress

In the process of shelling, the stress of the inner drum is analysed. Table 5 shows the analysis of the variance of the maximum pressure of particles.

ANOVA of the model of Box-Benhnken design experiment **Table 5**

Error sources	Square sum	Error freedom	Mean square	*F* value	*P* value
Model	3.74×10^{5}	9	41497.71	18.93	4×10^{-4}
A	5658.36	1	5658.36	2.58	0.1522
B	1.23×10^{5}	1	1.23×105	56.23	$<10^{-4}$
C	1.40×10^{5}	1	1.40×105	63.96	$<10^{-4}$
AB	2126.59	1	2126.59	0.97	0.36
AC	4449.56	1	4449.56	2.03	0.20
BC	22422.07	1	22422.07	10.23	$<10^{-2}$
A^2	7124.41	1	7124.41	3.25	0.1
B^2	43885.37	1	43885.37	20.02	2.9×10^{-3}
C^2	17615.84	1	17615.84	8.04	0.03

Table 5
(continuation)

Error sources	Square sum	Error freedom	Mean square	*F* value	*P* value
Residual item	1534.86	7	2191.98		
Missing items	9782.56	3	3260.85	2.35	0.21
Pure error	5561.30	4	1390.32		
Summation	3.89×10^5	16			

Note: R^2=0.9605; R_1^2=0.9098; C.V.=9.19%; Adep Precision=14.29

The coefficient of variation of *C.V.* is 9.19%, which shows that the test has high reliability. The Adep Precision value of 14.29 indicates that the model is of high precision, which demonstrates that the test has high reliability and accuracy. The *P* value of the missing fitting term is higher than 0.05, indicating that the quadratic polynomial equation has a high degree of fitting. Equation (1) is the quadratic polynomial equation of the shell breaking rate with all factors.

$$Y = -11455.99 + 11.24A + 1486.73B + 337.45C + 0.46AB - 0.13AC - 14.97BC - 0.02A^2 - 102.09B^2 - 2.59C^2 \quad (1)$$

Fig. 3 shows the response of the shelling clearance amount. When the shelling clearance amount is fixed, the pressure of the inner drum increases with the increase of the filling amount. When the filling amount is constant, the pressure of the inner drum decreases with the increase of the clearance. When the clearance gap is between 5.0 mm and 6.0 mm, the pressure of the inner drum decreases slowly with the growth of the filling amount. When the shelling gap is between 6.0 mm and 7.0 mm, the pressure of the inner drum decreases faster with the rise of the filling amount.

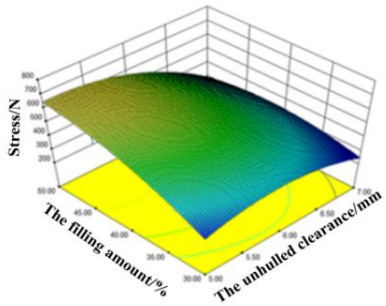

Fig. 3 - Response surface of interaction

Shelling removal rate results

According to Table 6, the variance analysis of the shelling pellet rate was performed. It can be seen that the coefficient of variation of C.V. is 0.89%, which proves that the experiment has a high degree of credibility. The determination coefficient R^2 and the adjusted determination coefficient R_1^2 are both close to 1, indicating that the fitting equation is highly reliable.

Equation (2) is the quadratic polynomial equation of the shell breaking rate with all factors.

$$Y = -60.97 + 0.46A + 7.07B + 3.59C - 0.02AB - 2.9\times10^{-3}AC - 0.18BC - 3.25\times10^{-4}A^2 - 0.27B^2 - 0.02C^2 \quad (2)$$

ANOVA of the model of Box-Benhnken designs experiment **Table 6**

Error sources	Square sum	Freedom	Mean square	*F* value	*P* value
Model	133.39	9	14.82	22.73	2×10^{-4}
A	11.62	1	11.62	17.82	3.9×10^{-3}
B	67.57	1	67.57	103.63	$<10^{-4}$
C	5.46	1	5.46	8.38	2.32×10^{-2}
AB	4.20	1	4.20	6.45	3.87×10^{-2}
AC	8.41	1	8.41	12.90	8.80×10^{-3}
BC	12.57	1	12.57	19.27	3.2×10^{-3}
A^2	2.77	1	2.77	4.25	7.82×10^{-2}
B^2	0.31	1	0.31	0.48	0.51
C^2	19.90	1	19.90	30.51	9×10^{-4}
Residual	4.56	7	0.65		
Missing items	1.94	3	0.65	0.98	0.48
Pure error	2.63	4	0.66		
Summation	137.95	16			

R^2=0.9669; R_1^2=0.9244; C.V.=0.89%; Adep Precision=19.38

P value of the model is less than 0.01, so all factors of the design test have a significant impact on the rate of shelling removal. The rotational speed, shelling clearance, and filling amount have a significant impact on the shelling rate. Among them, the shelling clearance has the most significant impact, followed by the rotational speed, and the filling amount is the smallest.

The interaction between rotational speed×filling amount and shelling gap×filling amount has a significant impact on the shelling removal rate. Among them, the influence of rotational speed×filling amount is greater than the rotational speed×shelling rate.

The shelling removal rate was set as the maximum value, and the optimal parameters were obtained. When the rotational speed was 350r/min, the shelling gap was 5.0 mm, and the filling amount was 40%.

Take the shelling clearance gap as 5.0 mm and analyse the interaction between the remaining two factors. Fig.4 (a) shows the effect analysis diagram of rotational speed×filling quantity. When the rotational speed was fixed, with the increase of the filling amount, the unshelled particles first increase and then decreased. As the filling amount was 40%, the castors shell broken. If the filling amount was fixed, the shell removal rate increased with the increase of rotational speed. When the filling amount was between 30% and 40%, the shelling rate rose rapidly with the rising of rotational speed. Furthermore, if the filling amount was between 40% and 50%, the shelling rate increased slowly with the increase of rotational speed.

As the drum rotational speed was 350 r/min, the interaction between the remaining two factors was analysed. Fig. 4 (b) shows the effect analysis diagram of the shelling clearance×filling amount. When the shelling clearance was fixed, with the increase of the filling amount, the unshelled particle firstly increased and then decreased. The peak value reached when the filling amount was 40%. When the filling amount was fixed, the rate of shell removal decreased with the increase of shelling gap.

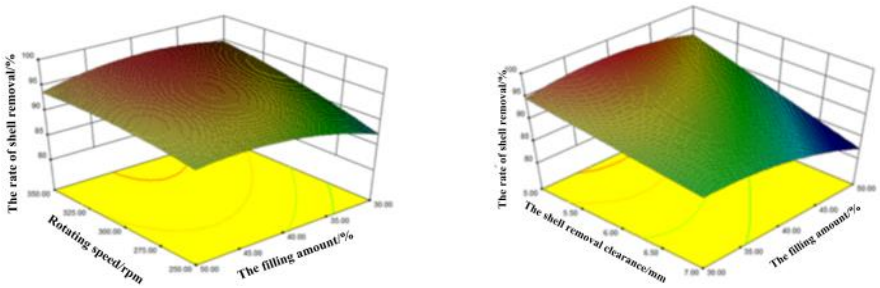

(a) *(b)*

Fig. 4 - Response surface of interaction

Single factor analysis of castor capsule shelling

Table 7 shows the effect of rotational speed on each result. With the increase of rotational speed, the force on the inner drum first increased from 509.34N to 533.14N, and then decreased to 456.15N. The shelling rate first increased from 91.23% to 91.28% and then decreased to 88.89%.

Influence of rotational speed on each result **Table 7**

Speed	Internal drum stress	Shelling rate
[r/min]	[N]	[%]
250	509.34	91.23
300	533.14	91.28
350	456.15	88.89

Table 8 shows the influence of the shelling clearance on each result. With the increase of the shelling clearance, the force of the inner drum decreased from 576.39N to 528.14N. The shelling rate decreased from 92.50% to 83.41%.

Influence of shelling gap on each result **Table 8**

Shelling gap	Internal drum stress	Shelling rate
[mm]	[N]	[%]
5	576.39	92.50
6	560.23	89.59
7	528.14	83.41

Table 9 shows the influence of the filling amount on each result. With the increase of the filling amount, the force on the inner roller first increased from 338.58N to 603.364N. The rate of shelling decreased from 91.00% to 90.05%.

Table 9

Influence of loading on each result

Filling capacity	Maximum pressure	Maximum speed	Inner drum force	Shelling rate
[%]	[N]	[m/s]	[N]	[%]
30	55.86	12.99	338.58	91.00
40	68.67	12.14	543.61	90.86
50	76.93	10.86	603.36	90.05

Size optimization of shelling parts

When the parameters of the inner and outer drum change, the volume of the unshelled drum will change. Fig. 5 shows the dimensions of the shelling parts.

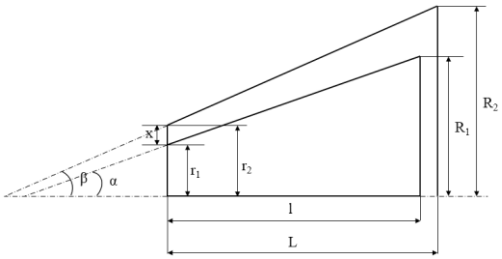

Fig. 5 - Dimensions of shelled parts

In Fig.5, l and L are the length of the inner and outer drum; r_1 and r_2 are the radius of the small end of the inner and outer drum respectively. R_1 and R_2 are respectively the large end radius of the inner and outer drum; x is the shelling clearance; α and β are inside and outside the shelling drum cone angle respectively.

The volume change is shown in equation (3):

$$\begin{cases} \Delta V = V_2 - V_1 \\ V_1 = \frac{1}{3}\pi l(r_1^2 + r_1 R_1 + R_1^2) \\ V_2 = \frac{1}{3}\pi L(r_2^2 + r_2 R_2 + R_2^2) \\ R_1 = r_1 + l\tan\alpha \\ r_2 = r_1 + x \\ R_2 = r_2 + L\tan\beta \\ \alpha < \beta \end{cases} \quad (3)$$

Where: ΔV for hulling chamber volume, mm^3.

V_1 and V_2 are respectively the volumes of the inner and outer drum, mm^3;

l and L is the length of the inner and outer drum, mm;

r_1 and r_2 are respectively the radius of the small end of the inner and outer drum, mm;

R_1 and R_2 are respectively the radius of the large end of the inner and outer drum, mm;

x is the shelling clearance, mm;

α and β, inside and outside the drum cone angle, respectively, °.

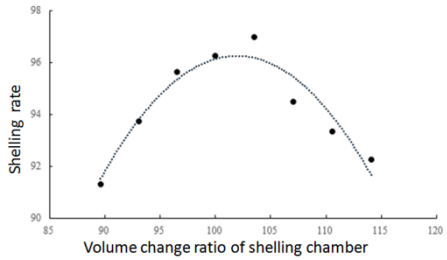

Fig. 6 - Relationship of shelling room volume changes and shelling rate

When the shelling rate was the highest, the rotational speed was 350r/min, the shelling gap was 5.0 mm, the volume of the outer drum platform was $8.06\times10^{-2}mm^3$, and the volume of the shell removal chamber was $2.40\times10^{-2}mm^3$. Fig. 6 shows the relationship between the volume change of the shelling chamber and the rate of shelling.

The fitting equation can be obtained as equation (4).

$$y = 0.03x^2 + 6.35x + 227.20 \quad (4)$$

As can be seen from Fig.6, with the increase of the volume of the shelling chamber, the shelling rate increased first and then decreased. From equation (3), it can be seen that the volume change of the shelling removal drum is 105.83% to that of the original shelling inner drum. That is, when the volume of the original shell removal drum is increased by 5.83%, the maximum value of the shelling clearance rate is 96.03%. As the inner drum is the main shelling part, its size parameters are optimized, while the outer drum parameters are fixed. The shelling gap is 5.0mm, so the small end radius of the inner drum is set. By changing the cone angle and length of the inner drum, the volume of the shell removal drum increases by 5.83%. By calculation, the volume of the internal drum is $5.61\times10^{-2}m^3$.

Shelling machine design

Based on the parameter setting of the simulation shelling model, the shelling machine was designed. We take shelling clearance and filling amount as the factors in the experiment. The experiment working conditions was compared with the simulation results. Shelling interval and filling quantity are factors, furthermore the damage rate and productivity are as an index. The experiment results were compared with the simulation results. Fig.7 is the schematic diagram of the whole machine, Fig.8 is the schematic diagram of the inner drum. Table.10 shows the adjustment parameters of the shelling machine.

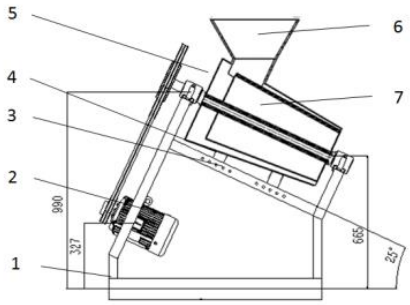

Fig. 7 - Schematic diagram of shelling machine

1. Motor; 2. Base frame; 3. Adjustment hole; 4. Adjustment arm; 5. Outer drum; 6. Feed hopper; 7. Inner drum

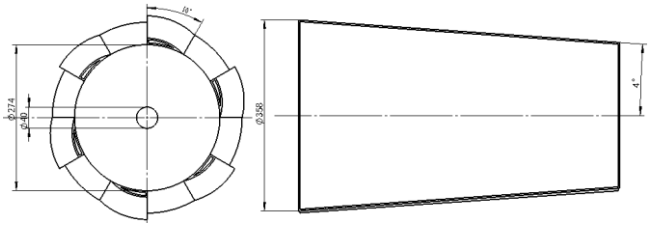

Fig. 8 - Schematic diagram of the inner drum

Table 10

Adjustment parameters of test bench

Adjustment parameters	Rotational speed	Shell clearance	Fill the quantity
Adjustment mode	Frequency converter control	The drum moves forward and backwards on its axis	Input material quality

Test methods and instruments

The rotational speed of the inner drum, the clearance clearance, and the filling amount are the test factors, while the shelling rate, damage rate, and productivity are the test indicators. The rotational speed of the inner drum is changed through the frequency converter, the position of the outer drum is adjusted to change the shelling clearance, and the amount of feed is adapted to fit the filling amount.

The camera aims at the observation window and records the status of materials in the drum. Table 11 shows the test factor level setting.

Before each group of experiments, the total amount of feed was weighed. After the experiment, the castor capsules were selected and weighed, then the rate of shelling and damage is:

$$C_1 = \frac{W_a+W_b}{W_a+W_b+W_c} \quad (5)$$

$$C_2 = \frac{W_b}{W_a+W_b} \quad (6)$$

$$C_3 = \frac{W_a+W_b+W_c}{T} \quad (7)$$

Where, C_1 is the shelling rate, %; C_2 is the damage rate, %; C_3 is the productivity, kg/h;

W_a is castor bean seed weight, kg; W_b is the seed weight of damaged castor bean, kg;

W_c refers to the unpurified castor bean seed weight, kg;

T is the working time, h.

Table 11

Test factor level setting

Level	A Rotational speed	B Shelling gap	C Filling amount
	[r/min]	[mm]	[%]
-1	250	5	30
0	300	6	40
1	350	7	50

The experimental material was castor Tongbi 11. When the moisture content of the material is 14.2%, the shelling experiment is carried out. Fig.9 shows the testbed for castor shelling.

Fig. 9 - Castor Shelling Test Bed

1. Host; 2. Motor; 3. Light source; 4. Adjustment hole; 5. Frequency converter; 6. Adjustment arm; 7. Shelling drum; 8. Feeding hopper; 9. Observation window; 10. Frame; 11. High speed Camera

Analysis of test results

Table 12 shows the experiment results. It can be seen that for the shelling rate, the rotational speed is 350r/min, the shelling gap is 5.0mm, and the filling amount is 30% at the optimal level. For the damage rate, the optimal level is 250r/min, the optimal level is 7.0mm, and the optimal level is 50% of the filling amount. For productivity, the optimal speed is 350r/min, the shelling gap is 7.0mm, and the filling amount is 50%.

Experiment results **Table 12**

Test number	A	B	C	Shelling rate	Damage rate	Productivity
				[%]	[%]	[kg/h]
1	-1	-1	-1	90.56	3.06	336.73
2	-1	0	0	86.72	2.82	362.49
3	-1	1	1	85.69	2.64	386.24
4	0	-1	0	90.51	2.93	375.26
5	0	0	1	90.68	3.16	382.46
6	0	1	-1	88.21	2.71	428.72
7	1	-1	1	91.82	3.22	456.75
8	1	0	-1	94.25	3.49	395.89
9	1	1	0	87.28	2.67	483.21

(a) Intact castor seeds

(b) Undershelled castor seeds

(c) Damaged castor seeds

Fig. 10 - Shelling effect of the testbed

Comparison of shelling rate

It can be seen that the influences of rotational speed and shelling clearance on the shelling rate are both higher than the filling amount. Table 13 shows the comparison of simulation and test results of the shelling removal rate. It can be seen that the differences between simulation results and the measured results are small, with the difference ratio within 9%. The significance order of each factor obtained by simulation is the shelling gap, rotational speed, and filling amount. The significance order of each factor obtained by the experiment is the shelling gap, rotational speed, and filling amount. They are in the same order. The optimal combination obtained by the simulation is 350r/min, the shelling gap is 5.0mm, and the filling amount is 40%. The optimal combination obtained by the experiment is 350r/min, shelling gap is 5.0mm, and the filling amount is 30%. Among them, the speed and the shelling gap are incredibly significant factors, and the filling amount is substantial factor.

Table 13

Comparison between simulation and experiment results on shelling rate

No.		1	2	3	4	5	6	7	8	9
Simulation results	**[%]**	93.29	91.36	93.17	96.24	94.23	89.47	87.96	88.32	93.17
Experiment results	**[%]**	90.56	86.72	85.69	90.51	90.68	88.21	91.82	94.25	87.28
Difference		3.01	5.35	8.73	6.33	3.91	1.43	4.20	6.29	6.75

CONCLUSIONS

(1) The shelling gap and the filling amount have a significant impact on the pressure of the inner drum, while the rotational speed has no significant impact on the pressure of the inner drum. With the increase of rotational speed, the force on the inner drum first increased from 509.34N to 533.14N, and then decreased to 456.15N. With the increase of the shelling clearance, the force of the inner roller first increased from 338.58N to 603.364N and the rate of shelling increased from 91% to 90.05%.

(2) The size of the shelling drum parameters was optimized. In the conditions of highest shelling rate, the size parameter was obtained. The optimized shelling drum cone angle was 4.5 ° and the drum length was 605.0 mm. Using this group of size parameters for simulation analysis, the shelling rate was 96.42%. There was a difference of 0.39% from the fitting value.

(3) The accuracy of the simulation model is verified on the shelling machine. The shelling clearance was significantly affected by the rotational speed, shelling rate, and filling amount. The damage rate was significantly affected by the rotational speed and shelling gap. By comparing the shelling rate, it can be seen that the difference ratio between the simulation result and the test result is 8.73% at the maximum and 1.43% at the minimum. The optimal parameter combination obtained by simulation was the rotational speed of 350r/min, the shelling gap of 5.0mm, and the filling amount of 40%. The optimal parameter combination obtained by experiment was the rotational speed of 350.0r/min, the shelling gap of 5.0mm, and the filling amount of 30%.

ACKNOWLEDGEMENT

This research was supported by the National Natural Science Foundation of China, China (51457312), the authors thank relevant scholars for their assistance in the literature.

REFERENCES

[1] Ali N. L., Farzad J., Rashid G., (2013), Physical and mechanical properties of castor seed. *Quality Assurance and Safety of Crops and Foods*, Vol. 4, Issue 05, pp.29-32;

[2] Bo Y.L., Rosnah S., Robiah Y., (2014), Development and testing of a Jatropha fruit shelling process for shell-free kernel recovery in biodiesel production. *Biosystems Engineering*, Vol.121, pp.46-55;
[3] Boyuan L., Shamsudin R., Baharudin B.T.H.T. et al., (2015), A review of processing and machinery for Jatropha curcas L. fruits and seeds in biodiesel production: harvesting, shelling, pre-treatment and storage. *Renewable & Sustainable Energy Reviews*, Vol. 52, Issue 03, pp.991-1002;
[4] Coetzee C J., (2016), Calibration of the discrete element method and the effect of particle shape. *Powder Technology*, Vol. 297, pp.75-139;
[5] Dun G.Q., Chen H.T., Zha S.H. (2016), Parameter optimization and validation of soybean cell wheel seeding plate type-hole based on EDEM. *Soybean Science*, Vol. 35, Issue 05, pp.204-214;
[6] Fang H.M., Ji C.Y., Zhang Q.Y. et al., (2016), Force analysis of rotary blade based on distinct element method. *Transactions of the Chinese Society of Agricultural Engineering*, Vol. 32, Issue 21, pp.54-58;
[7] Hao W.J., Tian Q.J., Cai Y.G., (2010), Numerical analysis on effect of media-to-material ratio on working performance of ball mill. *Mining Machinery*, Vol. 38, Issue 23, pp.72-75;
[8] Hou J.M., Yang Y., Zhu H.J., Hu W.X., (2020), Experiment on impact damage of castor capsule and its influence factors optimization. *INMATEH-Agricultural Engineering*, Vol. 61, Issue 3, pp.87-96. https://doi.org/10.35633/inmateh-61-10
[9] Huang Z.H., Cheng X.X., Li C.Z. et al., (2013), Mechanical model and major influential factors of breaking castor shell. *Journal of Shenyang Agricultural University*, Vol. 44, Issue 02, pp.185-189;
[10] Jia H.L., Chen Y.L., Zhao J.L. et al., (2018), Design and experiment of pneumatic-mechanical combined precision metering device for soybean. *Transactions of the Chinese Society of Agricultural Machinery*, Vol. 49, Issue 04, pp.75-139;
[11] Li J.Q., Zhu G.L., Wu G.L. et al., (2004), Correlation and path analysis between seed oil content and major quantitative characters in castor. *Chinese journal of oil crop sciences*, Vol. 26, Issue 2, pp.43-46;
[12] Li K.Y., Tong X., Li Z.F. et al., (2017), Research on parameters of ball mill's trapezoidal liner based on DEM-FEM coupling approach. *Journal of Fujian University of Technology*, Vol.16, Issue 65, pp.23-527;
[13] Liu R.K., Cheng X.X., Xiao Z.H. et al., (2015), Finite element simulation on mechanical property of castor capsule during husking. *Journal of the Chinese Cereals and Oils Association*, Vol.30, Issue 5, pp.62-66;
[14] Mehrdad P., Colin H., Mojtaba G. et al., (2016), Effect of particle shape on flow in discrete element method simulation of a rotary batch seed coater [J]. *Powder Technology*, Vol. 296, pp.29-36;
[15] Sebastian R., Shkelqim K., Joachim M., (2015), Influence of physical properties of Jatropha curcas. Seeds on shelling performance using a modified disc mill. *Industrial Crops and Products*, Vol. 77, pp.1053-1062;
[16] Shi S., Zhang D.X., Yang L. et al., (2015), Simulation and verification of seed-filling performance of pneumatic-combined holes maize precision seed-metering device based on EDEM. *Transactions of the Chinese Society of Agricultural Engineering*, Vol. 31, Issue 03, pp.62-69;
[17] Sinnott M.D., Cleary P.W., Morrision R.D., (2017), Combined DEM and SPH simulation of overflow ball mill discharge and trammel flow. *Minerals Engineering*, Vol.108, pp.93-108;
[18] Sun S.S., Dong W.M., Wang Z.R. et al., (2018), The design of wave liner for SAG mill based on EDEM and ANSYS coupling method. *Mining & Metallurgy*, Vol. 17, Issue 06, pp.830-839;
[19] Wang X.L., Hu H., Wang Q.J. et al., (2017), Calibration method of soil contact characteristic parameters based on DEM theory. *Transactions of the Chinese Society of Agricultural Machinery*, Vol. 48, Issue12, pp.78-85;
[20] Wang Z.B., Xu W.J., Li X.W. et al., (2015), Test on the mechanical properties of kenaf capsule. *Journal of Chinese Agricultural Mechanization*, Vol. 36, Issue 06, pp.136-138;
[21] Xiong P.Y, Yang Z., Sun Z.Q. et al., (2018), Simulation analysis and experiment for three-axis working resistances of rotary blade based on discrete element method. *Transactions of the Chinese Society of Agricultural Engineering*, Vol. 34, Issue 18, pp.113-121;
[22] Xiong P.Y., Yang Z., Sun Z.Q., et al., (2017), Experiment on three-axis working resistances of rotary blade and working parameters optimization. *Transactions of the Chinese Society of Agricultural Engineering*, Vol. 33, Issue 19, pp.51-58;
[23] Zhao S.H., Zhou Y., Liu H.J. et al., (2016), Design of reseed shift speed system of scoop-type metering device of corn. *Transactions of the Chinese Society of Agricultural Machinery*, Vol.47, Issue 12, pp.38-44.